



Shear Banding in Binary Cu-Zr Metallic Glass: Comparison of the G-Phase With L-Phase

Yidi Shen¹, William L. Johnson^{2*}, Konrad Samwer^{2,3}, Sydney L. Corona², William A. Goddard^{4*†} and Qi An^{1*}

¹Department of Chemical and Materials Engineering, University of Nevada-Reno, Reno, NV, United States, ²Department of Materials Science, California Institute of Technology, Pasadena, CA, United States, ³I. Physikalisches Institut, University of Goettingen, Goettingen, Germany, ⁴Materials and Process Simulation Center, California Institute of Technology, Pasadena, CA, United States

OPEN ACCESS

Edited by:

Yue Fan,
University of Michigan, United States

Reviewed by:

Bin Wu,
Beijing Normal University, China
Kostya Trachenko,
Queen Mary University of London,
United Kingdom

*Correspondence:

William L. Johnson
wj@caltech.edu
William A. Goddard
wag@caltech.edu
Qi An
qia@unr.edu

†ORCID:

William A. Goddard
orcid.org/0000-0003-0097-5716

Specialty section:

This article was submitted to
Computational Materials Science,
a section of the journal
Frontiers in Materials

Received: 28 February 2022

Accepted: 31 March 2022

Published: 14 April 2022

Citation:

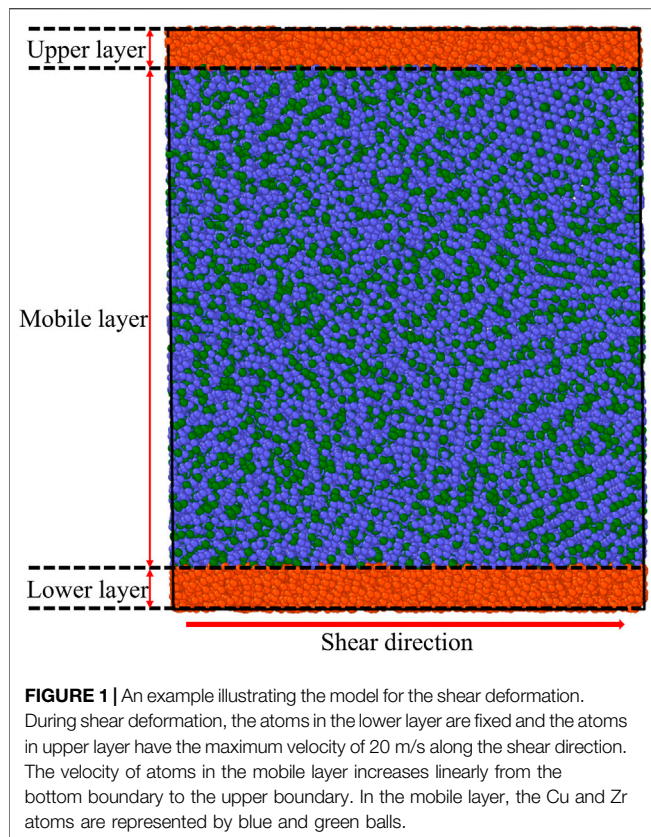
Shen Y, Johnson WL, Samwer K, Corona SL, Goddard WA and An Q (2022) Shear Banding in Binary Cu-Zr Metallic Glass: Comparison of the G-Phase With L-Phase. *Front. Mater.* 9:886788. doi: 10.3389/fmats.2022.886788

We identified two glass phases formed in three undercooled liquids of elemental Ag, binary Cu-Ag, and binary Cu-Zr alloys using molecular dynamics (MD) simulations: 1) The homogeneous L-phase arises from quenching quickly from high temperature liquid. 2) The heterogeneous solid-like G-phase arises from the isothermal equilibration at temperatures below the melting point. The G-phase exhibits a core-shell structure with the ordered cores surrounded by percolating liquid-like shells. The distinguishable structures between these two phases are expected to different mechanical behavior. The present study reports MD simulations to compare the shear deformation of these two phases in binary Cu₂Zr system. At room temperature, the G-phase exhibits a higher critical stress, a higher critical strain, and higher shear modulus than the L-phase, suggesting that the G-phase has improved strength and rigidity compared to the homogeneous L-phase. The plastic yielding mechanism of both the G-phase and L-phase is accompanied by shear band formation. However, the formation of shear band in G-phase is confined by the cores to a highly localized region and characterized by local mechanical melting. In contrast, the shear band in L-phase exhibits greater width and much more homogenous character. We conclude that the mechanical properties of a metallic glass will vary significantly according to the type of glassy phase formed during processing.

Keywords: metallic glass, plastic flow, shear deformation, MD, shear band, baushinger effect

INTRODUCTION

The mechanical properties of bulk metallic glasses (BMGs) have stimulated much interest due to such outstanding properties as high strength, large elastic strain limit, and good fracture toughness. However, the BMGs normally show low plasticity at room temperature, which limits extended applications (Gu et al., 2007; Li et al., 2013; Yang et al., 2019; Wu et al., 2021). The low plasticity originates from the unique deformation mechanism under loading, which is different from typical crystalline metals. BMGs tend to form highly localized shear bands due to the lack of dislocation systems and grain boundary structures (Pekarskaya et al., 2001; Yang et al., 2005; Schuh et al., 2007; Greer et al., 2013). These shear bands are much softer and more susceptible to subsequent flow than surrounding regions (Greer et al., 2013). Thus, plastic strains are localized within the shear bands while regions outside the shear bands deform elastically, which leads to the low global plasticity of BMGs (Klaumünzer et al., 2011; Tang et al., 2016). The soft shear bands have been widely observed in

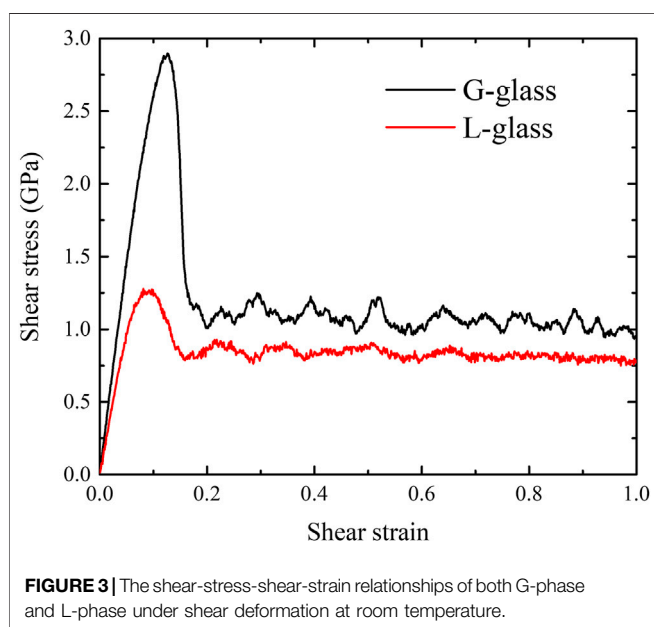
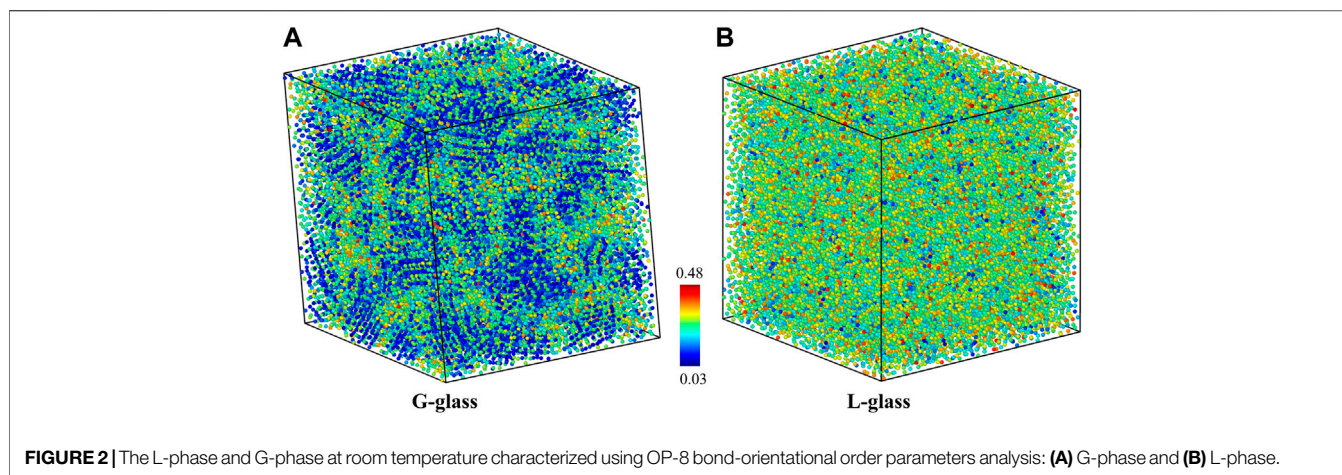


previous studies. For example, a single shear band in Zr-based BMGs has been isolated in a recent experimental study (Maaß et al., 2014). Even though the width of the shear band is of the order of some nanometers, the region showing structural softening due to the shear band has micrometer width. Thus, to understand and improve the mechanical properties for future engineering applications, it is essential to understand the mechanism of shear band formation.

Many studies have focused on understanding the failure mechanism and improving the mechanical properties of various BMG systems. Regarding the failure mechanism, it was proposed that the shear bands arise from the generation of free volume around the atoms to facilitate atomic motion and nucleating shear bands (Yang et al., 2005; Spaepen, 2006; Dai and Bai, 2008; Tang et al., 2016). In addition, adiabatic heating and softening is reported as another factor for localization of plasticity in BMGs. Local heating beyond glass transition temperature produces thermal softening, resulting in rapid shear band propagation and structural failure in BMGs (Lewandowski and Greer, 2006; Yang et al., 2006; Dai and Bai, 2008; Wang et al., 2015). Regarding the improvement of mechanical properties, several approaches have been developed to improve the global plasticity of BMGs at room temperature. This includes structure modifications (Hays et al., 2000; Szuëcs et al., 2001; Schroers and Johnson, 2004; Lee et al., 2006; Liu et al., 2007; Chen et al., 2008), elastostatic compression (Lee et al., 2008), and ion irradiation (Ke et al., 2011). For example, a

family of BMGs consisting of ZrCuNiAl were synthesized by choosing the composition to maximize the Poisson ratio (Liu et al., 2007). The ZrCuNiAl BMGs can undergo a true strain in compression as large as 160% without failure. TEM investigations on the microstructure of BMG composites indicate that these super plastic BMGs are composed of alternating hard regions and soft regions. Consequently, the shear transformation zones (STZ) prefer to activate in soft regions leading to numerous shear bands under loading. Propagation of the shear bands is arrested by hard regions, which encourages shear-band multiplication. Multiplication of the shear bands assists the enhanced global plasticity in the BMG composites.

The mechanical properties of BMGs are expected to be related to the local atomistic structure. In our recent MD simulations, we identified two glass phases in both elementary Ag and binary (Ag-Cu and Zr-Cu) liquids (An et al., 2020a; 2020b, 2021, 2022). When the metallic liquids are ultrafast quenched to room temperature (quench rate: $\sim 10^{12}$ K/s), the homogeneous liquid-like L-phase glass forms. In contrast, if the metallic liquid is quenched to intermediate temperatures below melting temperature, it evolves isothermally to the heterogeneous solid-like G-phase glass through a first order freezing transition. Unlike the homogenous L-phase, the G-phase possesses local core regions with crystalline-like short-range order surrounded by a liquid-like matrix. In particular, for Ag and Cu-Ag alloys, the core regions of the G-phase are mainly composed of crystalline-like FCC + HCP short range order with a heterogeneity correlation length scale $\Lambda \sim 4$ nm in pure Ag metals decreasing to $\Lambda \sim 2$ nm in the eutectic Ag-Cu system (An et al., 2020b). For Cu-Zr alloy, the core regions of G-phase show icosahedral short-range order, with correlation length Λ in the range of 1.5–1.8 nm (An et al., 2022). We also calculated the shear modulus and viscosity of both G-phase and L-phases from MD simulations. The G-phase has much higher elastic modulus and viscosity compared to the L-phase, suggesting the G phase shows greater elastic rigidity (An et al., 2020a; 2020b, 2022). Besides, a recent theoretical study shows formation of a partially crystallized glass phase in Cu_2Zr metallic liquid when isothermally holding at 950 K. This ordered state exhibits icosahedral structural character, which is similar to the G-phase in our study (Yue et al., 2020). Evidence for the existence of these two glass phases in BMG forming alloys has also been reported in the recent experimental studies. In the ultra-fragile Pt-Cu-P ternary alloy system, the glass transition evolves to an apparent first-order melting transition with varying composition (Na et al., 2020). This study suggests the existence of two amorphous glass phase: a high temperature disordered liquid-like glassy L-phase and a configurationally ordered lower temperature solid-like G-phase glasses. The G-phase like metallic glacial glass (MGG) was synthesized by a first order transformation of an initially quenched metallic glass phase (MG) that was reheated into the supercooled liquid of a $\text{La}_{32.5}\text{Ce}_{32.5}\text{Co}_{25}\text{Al}_{10}$ alloy (Shen et al., 2020). The MGG-phase exhibits a first-order melting-like transition to the disordered liquid phase upon subsequent rapid



heating. The hardness of the MGG phase is 20% higher compared to the initially quenched metallic glass (MG), providing further evidence of two distinct glass/liquid phases.

In the present study, we focus on the binary Cu_2Zr system and perform MD simulations to examine shear deformation behavior of both the L-phase and the G-phase at room temperature. Our simulations show that the critical shear stress and shear modulus of the G-phase (2.82 GPa for critical shear stress and 29.97 GPa for shear modulus) are both much greater than those of the L-phase (1.25 GPa for critical shear stress and 17.93 GPa for shear modulus). This suggests that the G-phase is stronger and exhibits greater rigidity compared to the L-phase. In addition, the G-phase has a larger critical shear strain (0.15) than that of L-phase (0.10). Thus, the G-phase is both stiffer and stronger than L-phase. Further analysis of the yielding mechanism indicates that shear strain localization (shear band formation) occurs for

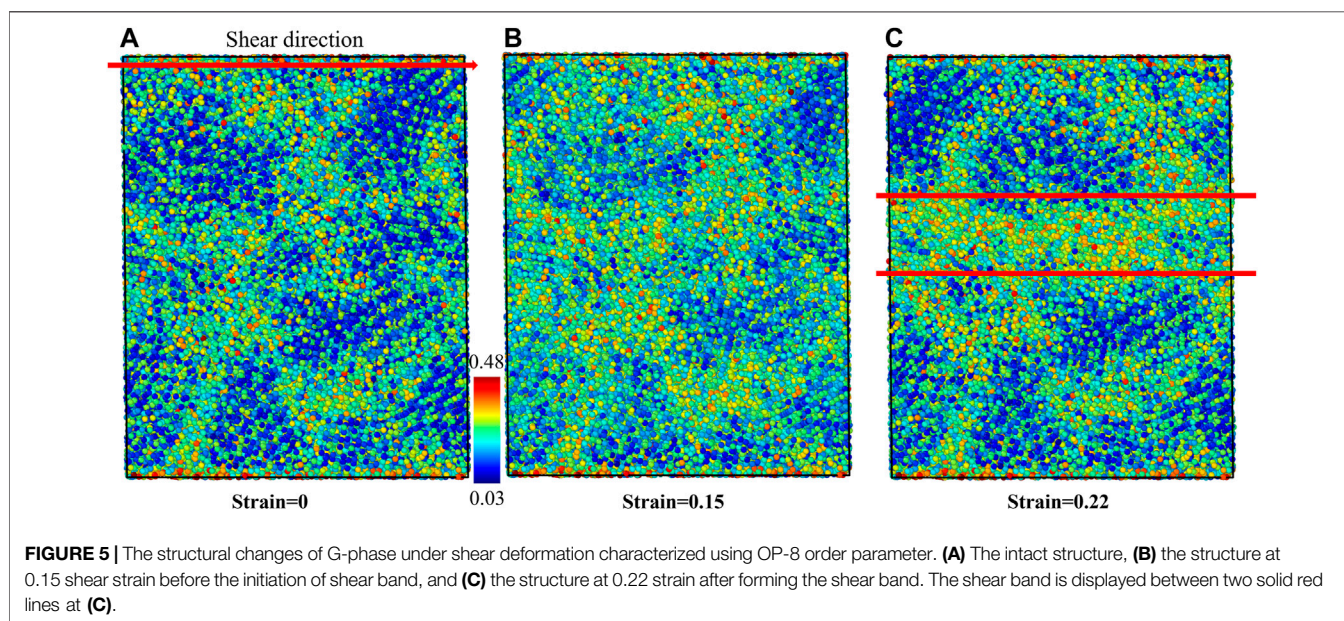
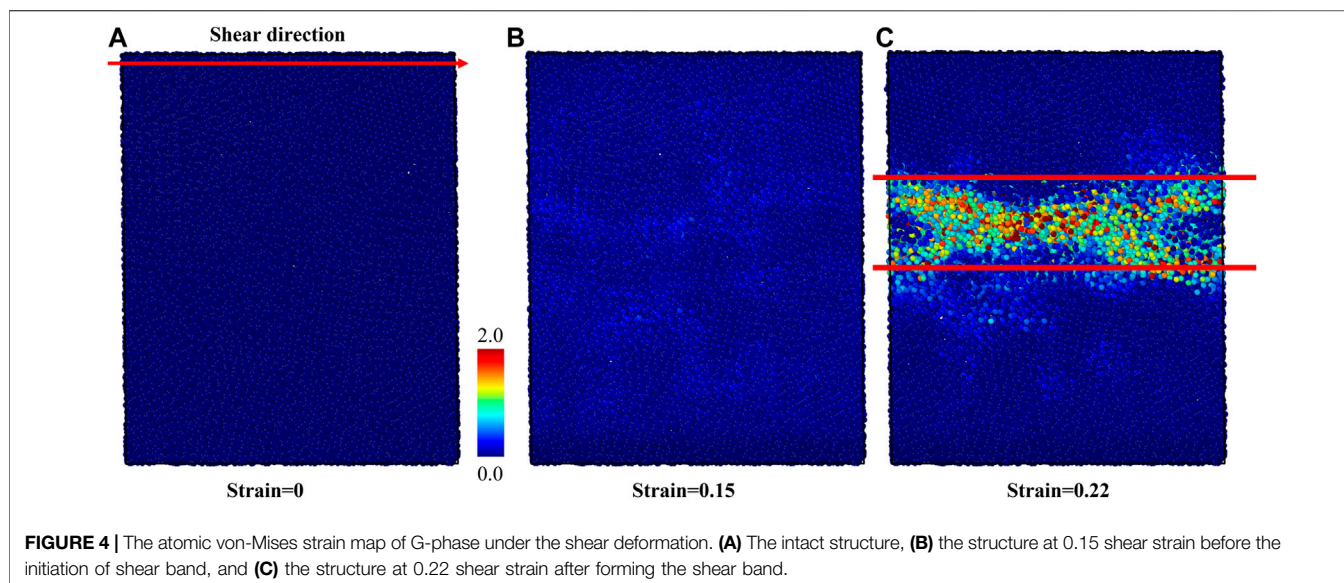
both G-phase and L-phases, following initial yielding. Within the localized shear band, the ordered core regions of the G-phase appear to lose their icosahedral character during shear sliding, this suggests local mechanical melting within the shear band. In contrast, the L-phase exhibits much broader and more diffuse shear band apparently related to its more homogenous structural character. After G-phase and L-phase reaches their steady flow state, their response under following cyclic loading exhibits the Bauschinger effect. The reason might be that the atoms in soft shear band have higher mobility and less resistance to shear. The plastic deformation in these structures becomes dominated earlier compared to unsheared structures.

METHODS

Model Construction and MD Simulations

All MD simulations were performed using the LAMMPS code (Plimpton, 1995). Sheng's Cu-Zr embedded atom model (EAM) potential is applied in MD simulations to describe the interatomic interactions (Cheng et al., 2009). The velocity Verlet algorithm is used for integrating the equations of motion with a timestep of 1.0 fs in all simulations. Periodic boundary conditions (PBC) along all three directions are used to eliminate surface effects in all simulations except for the shear deformation.

The L-phase is obtained from ultrafast quenching, which is similar to our previous studies (An et al., 2021, 2022). Firstly, the liquid with 41,472 atoms is equilibrated at 2000 K using the NPT ensemble for 1 ns. Then, the liquid is quenched from 2000 K to room temperature with a high cooling rate of 2.125×10^{12} K/s. In contrast, the G-phase is produced by isothermal aging the supercooled liquid at 900 K for 750 ns, as discussed in our previous work (An et al., 2022). Then, the G-phase is quenched to room temperature using the same cooling rate as for the L-phase (2.125×10^{12} K/s). Next, both L-phase and G-phase are relaxed at room temperature for 16 and 1 ns using NPT dynamics until reaching equilibrium, respectively.

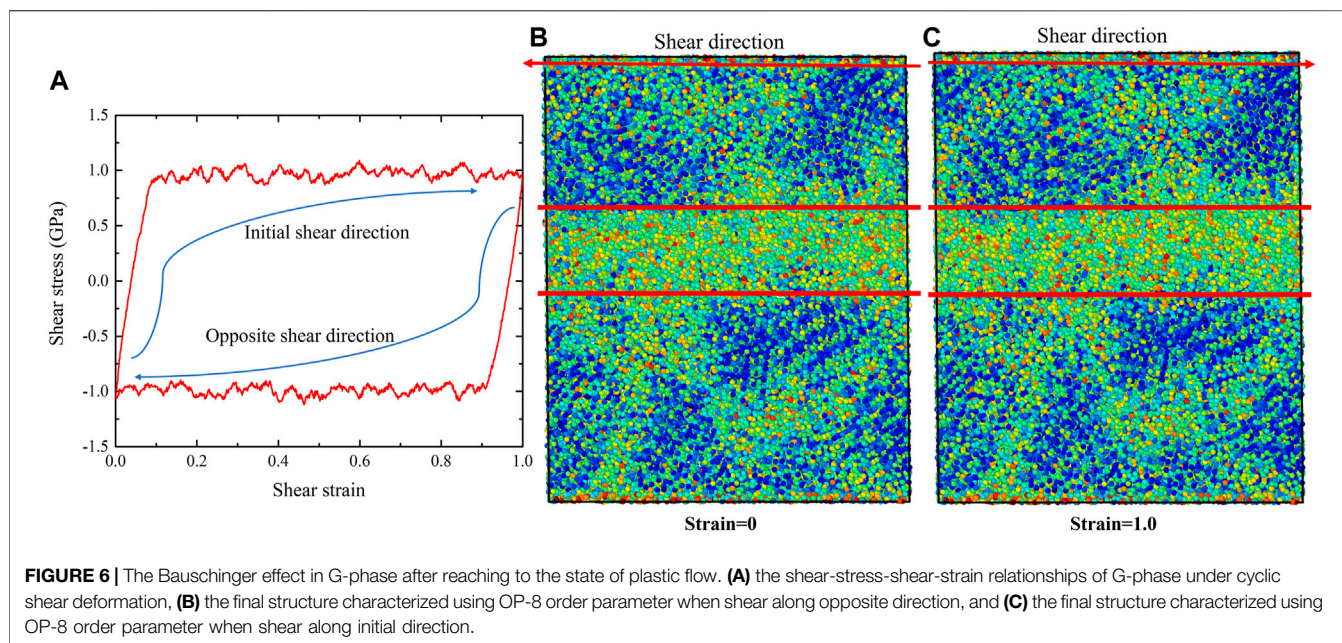


After obtaining the equilibrium L-phase and G-phase at room temperature, we apply finite shear rate deformations to examine their shear-induced failure processes. Here, our model is partitioned into three layers: the 0.5 nm thick immobile lower layer, the 0.5 nm thick immobile upper layer, and the mobile layer between these two layers with thickness of 7.6 nm for L-phase and 8.5 nm for G-phase, as shown in **Figure 1**. Then, a fixed velocity of 20 m/s along the shear direction is assigned to the atoms in the upper layer while the atoms in the lower layer are fixed. The velocities of atoms in the mobile layer increases from 0 to 20 m/s on top of their thermal velocities at 300 K. The corresponding engineering strain rate for all simulations is $\sim 0.002 \text{ ps}^{-1}$. We also consider lower strain rates of 0.0002 ps^{-1} and 0.00002 ps^{-1} to

investigate the effects of strain rate on shear deformation of both G-phase and L-phase. During the shear deformation, the NVE ensemble is applied to for the mobile atoms. Meanwhile, the velocities of two non-sheared directions for the atoms in the mobile layer is rescaled every 100fs to maintain 300 K for the system.

Plastic Yielding and Flow Mechanism Analysis: Atomic Structure Analysis and Bond-Orientational Order Parameter

To analyze the structural changes during shear band formation and steady state shear, we calculated the atomic von Mises strains



(Shimizu et al., 2007) using the software OVITO (Stukowski, 2010). The atomic von Mises strains are examined based on the particle displacement vectors of current atomistic configuration referenced to the initial structure (Shimizu et al., 2007; Tucker et al., 2011). A large von Mises strain suggests a large local atomic strain.

The local ordered structures during the shear deformation are analyzed using the bond-orientational order parameters (BOOP), q_l ($l = 2, 4, 6, 8, \dots$) (Steinhardt et al., 1983; Mickel et al., 2013). In BOOP, the q_l are sensitive to local atomic symmetries in the bond angles, which are compared to values for ideal lattices. This allows analysis of the atomic arrangements on the level of individual constituents. In this study, q_8 parameters were adopted to identify the structural change because they are sensitive to the icosahedral structure in the G-phase and the disordered structure in the L-phase (An et al., 2022). Note that the cut-off range of each atomic site relative to its neighboring atoms for both the atomic strain and the BOOP analysis is determined using the first minimum value following the first maximum of the radial distribution function.

RESULTS AND DISCUSSION

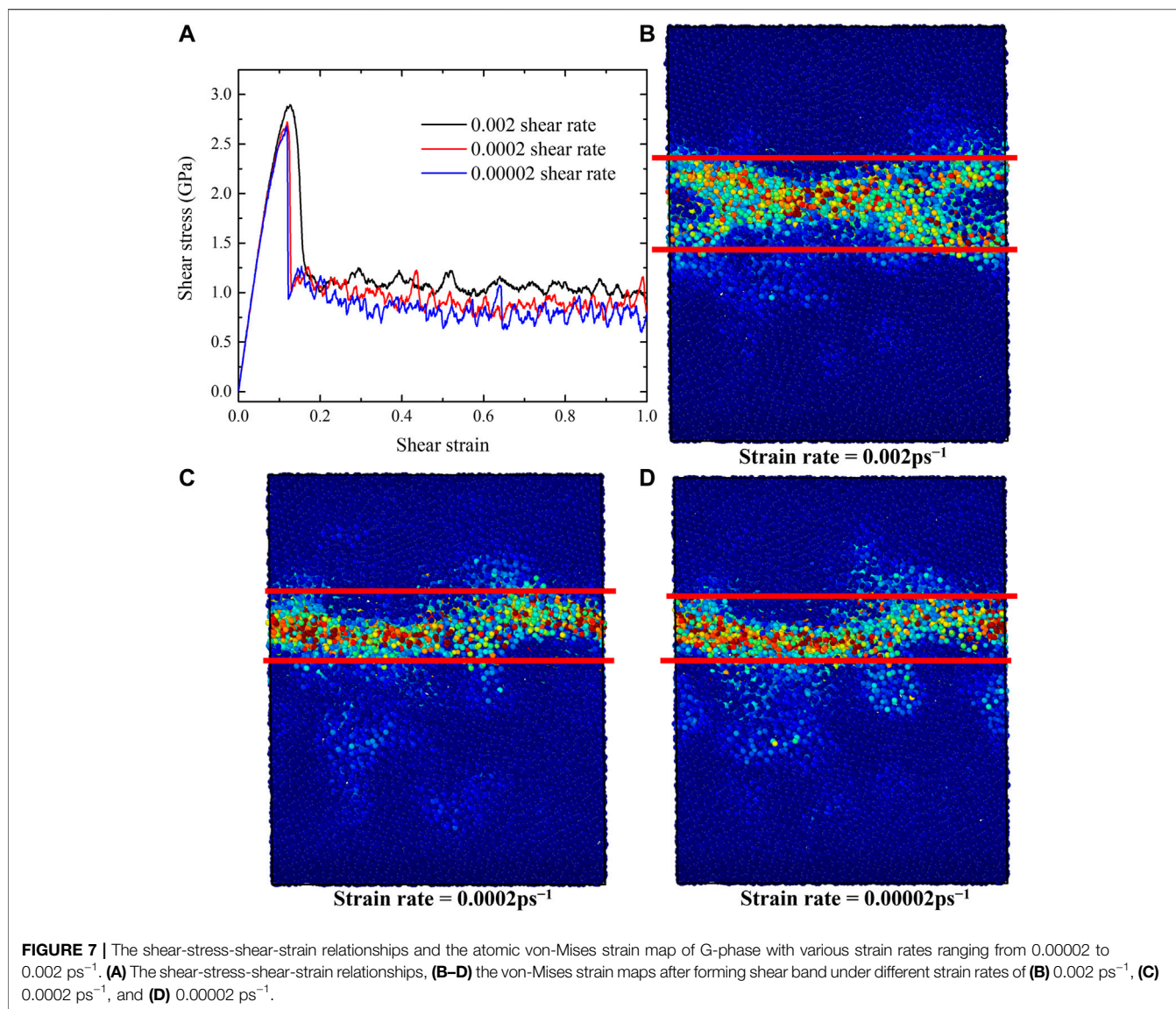
The Flow Mechanism of G-phase Under Shear Deformation

The local atomic structure of the G-phase at room temperature is characterized using BOOP analysis, as shown in **Figure 2A**. This structure shows a heterogeneous character being composed of two different configurational regions: a icosahedral-ordered core region with low OP-8 surrounded by a percolating liquid-like disordered matrix with high OP-8 (An et al., 2022).

We performed the shear deformation of G-phase at room temperature. The predicted shear-stress-shear-strain relationship

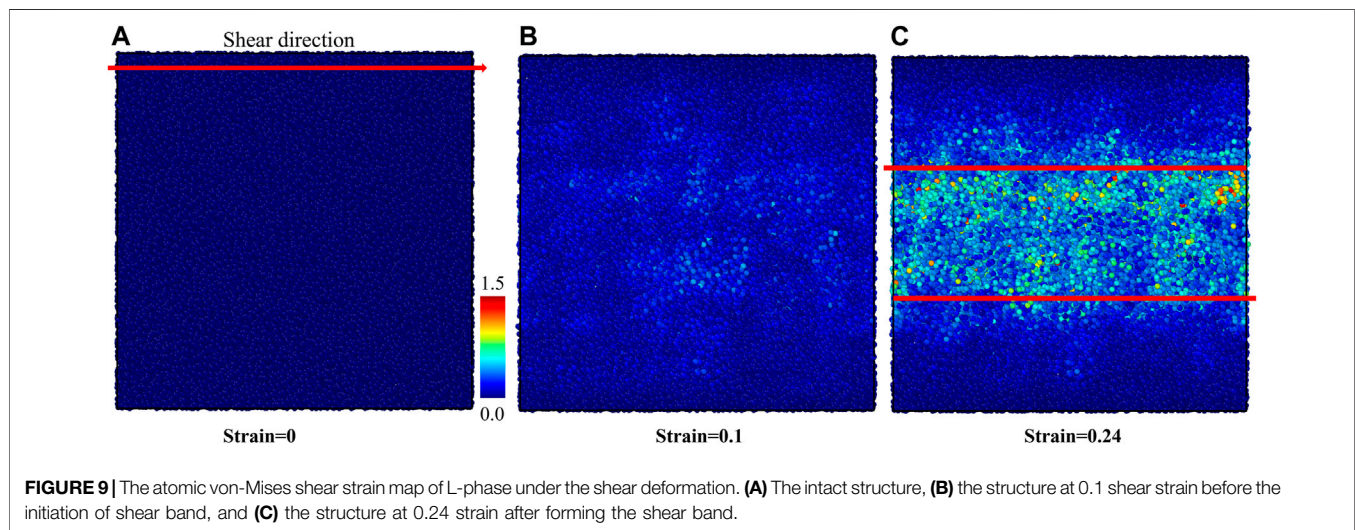
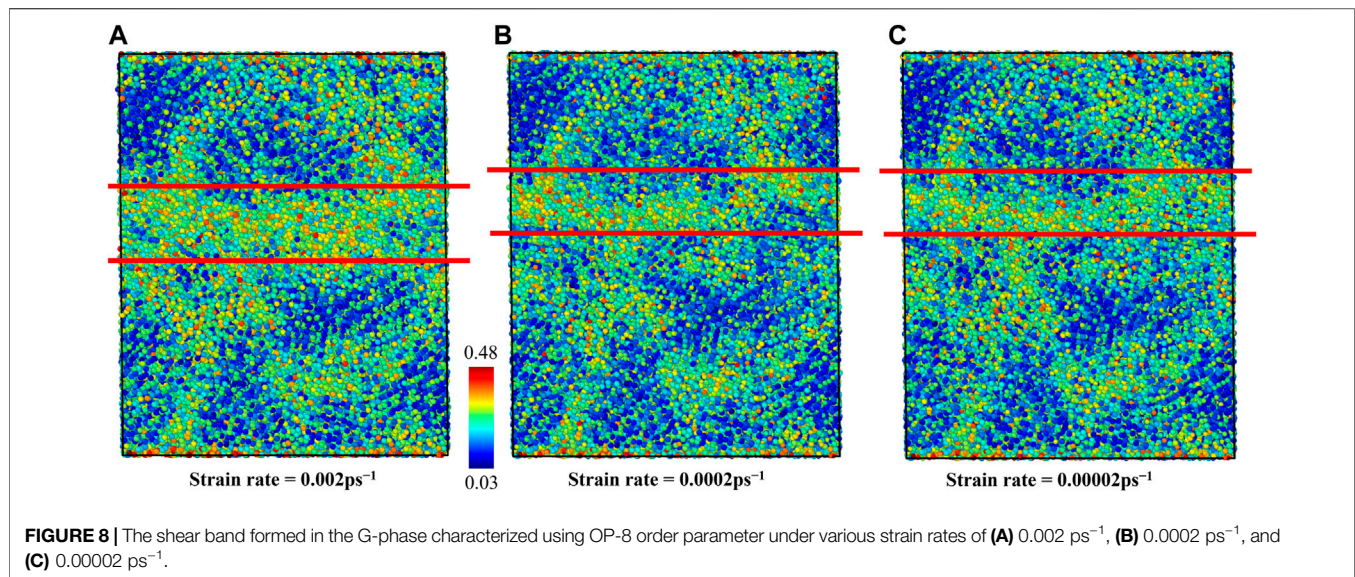
of the G-phase is shown in **Figure 3**. The predicted critical shear stress is 2.82 GPa at a shear strain of 0.15. Before the shear stress reaches its maximum value, the G-phase first undergoes an elastic deformation at a calculated shear modulus of 29.97 GPa. Then the shear stress reaches a peak followed by a continuous decrease from the maximum shear stress to ~ 1.0 GPa with an increase of shear strain up to 0.22, suggesting plastic flow in the G-phase. The flow behavior of the G-phase under shear deformation is shown in **Figure 4**. To analyze the plasticity mechanism, we display the atomic von Mises shear strain maps during shear deformation. **Figure 4A** shows the intact structure before shear. As the shear strain increases to 0.15, which corresponds to the peak shear stress of 2.82 GPa, the structure deforms elastically, as shown in **Figure 4B**. Note that the atoms in the core regions experience relatively smaller shear strain compared to the atoms in the surrounding disordered region up to 0.15 shear strain. As the shear strain increases further continuously, a shear band nucleates and then propagates along the shear direction, leading to relaxation of the overall shear stress as well as localization of the shear strain into a shear band. In particular, at 0.22 shear strain, a shear band having a width of ~ 3 nm propagates across the entire G-phase MD cell, which correlates with the stress drop to ~ 1.0 GPa, as shown in **Figure 4C**. Interestingly, the width of the formed shear band varies along the shear direction while a region with low atomic strain exists inside the shear band near the sample boundaries along the x -axis. This suggests that this shear band may actually be bifurcated.

To understand the plasticity mechanism of shear band sliding in the G-phase, the BOOP analysis was performed to investigate the evolution of locally ordered structures during shear band sliding. The OP-8 order parameters are adopted to examine the local structures during the shear deformation. The intact structure before shear is shown in **Figure 5A** in which the



core regions and surrounding disordered matrix regions can be clearly delineated. At 0.15 shear strain, the OP-8 values in the core regions begin to increase compared to the intact structure due to the evolving plastic shear strain, as shown in **Figure 5B**. However, not all core regions are deconstructed at this shear strain. As the global shear strain increases to 0.22, a shear band core with high OP-8 forms, which agrees with the atomic strain map, as shown in **Figure 5C**. More important, as strain increases, part of the core regions lying within the shear band transform from the ordered structure (low OP-8) to the disordered structure (high OP-8), suggesting that the shear band sliding in the G-phase arises from mechanical melting of these core regions. In addition, the plasticity is clearly localized and correlated with the results of OP-8 and is consistent with the results from atomic von-Mises strain. The nearby core region with a crystal-like local structure appears to block the propagation of the shear band.

After the G-phase reaches plastic-flow state at 1.0 shear strain, we then applied reversed shear strain to investigate its response under opposite loading condition. The obtained shear-stress-shear-strain relationship is shown in **Figure 6A**. During the shear deformation along reversed direction, the stress quickly decreases to 0 and then increases to the same absolute value of steady-state flow stress (~ 1.0 GPa). After G-phase reaches the plastic flow state again, we switched the shear direction one more time to the initial direction and further explored the plastic evolution of G-phase under cyclic loading. Similar to the response during the shear deformation along reversed direction, the shear stress quickly flips back and then shows a steady flow with the value of ~ 1.0 GPa, as shown in **Figure 6A**. This stress reversal under cyclic loading indicates the Bauschinger effect (Karmakar et al., 2010; Frahsa et al., 2013; Urata and Li, 2018; Patinet et al., 2020) in G-phase under pure shear deformation. In order to understand the origin of this

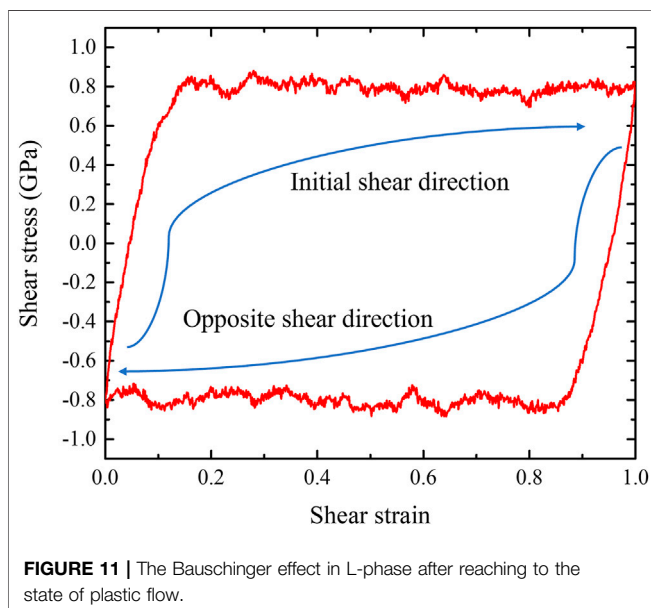
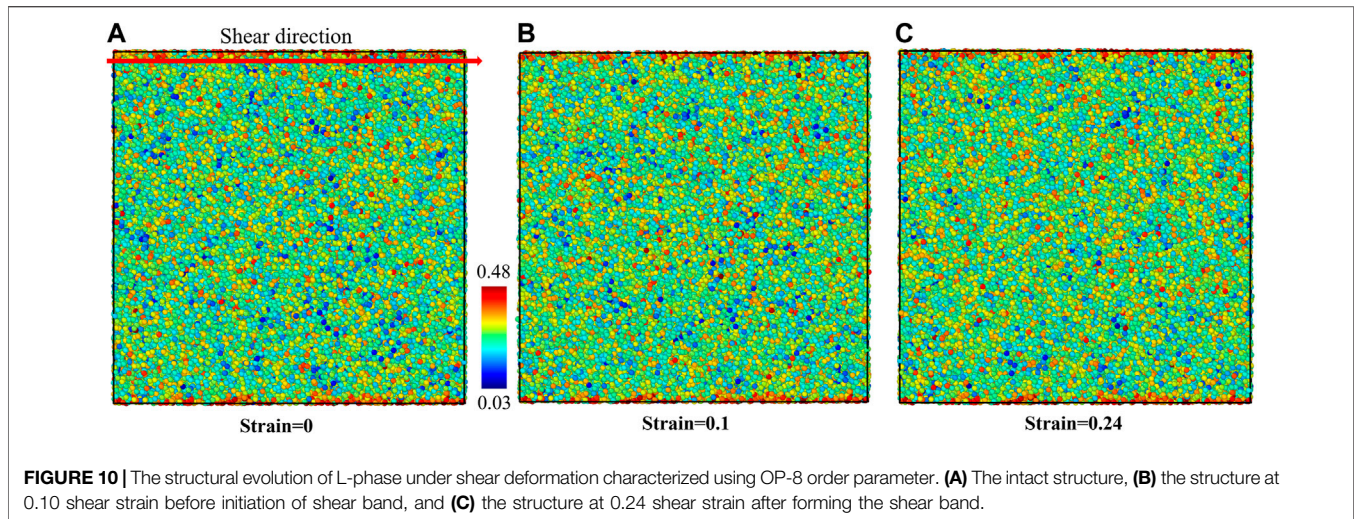


phenomenon, we then used OP-8 order parameters to examine the evolution of local structures. The structures at 0 and 1 shear strains, which correspond to the final structures when shear along both opposite and initial directions, are shown in **Figures 6B,C**. Compared to the structure after forming the shear band (**Figure 5C**) during the initial shear deformation, no obvious structural change is observed in these two structures. Thus, the Bauschinger effect for G-phase might be explained by the composite model (Pedersen et al., 1981; Sun et al., 2014). Under the initial loading, the formation of shear band suggests the existence of both the softer region (shear band) and the harder region (surrounding undeformed region) in plastic deformed G-phase (Greer et al., 2013). When loading is reversed, the atoms in the shear band have higher mobility and less resistance to shear than those in the surrounding regions (Sun et al., 2014). Therefore, the formed shear band can plastically

deform earlier than the initially unsheared structure, causing the Bauschinger effect.

From the results of both atomic strain and BOOP analyses, we conclude that the plastic flow mechanism of the G-phase under shear deformation arises from local mechanical melting of core regions within the operating of a shear band. In addition, the nearby icosahedral-ordered core regions apparently obstruct and deflect propagation of the shear band, causing additional localization of the shear band between surrounding core regions. After G-phase reaches plastic-flow state, it follows the plastic manner of Bauschinger effect under cyclic loading. This might result from the formed soft shear band that has less resistance to shear and can plastically deform earlier than initially unsheared structure.

Strain rate is an important factor for the shear deformation. To illustrate the strain rate effects, we considered two lower strain



rates of 0.0002 ps^{-1} and 0.00002 ps^{-1} for the G-phase. The shear-stress-shear-strain relationships obtained at various strain rates are shown in **Figure 7A**. When the strain rate decreases from 0.002 ps^{-1} to 0.0002 ps^{-1} , both the critical shear stress and shear strain before plastic flow decrease from 2.82 GPa and 2.42 GPa to 0.15 and 0.12, respectively. The steady flow stress also decreases from ~ 1.0 to 0.8 GPa. However, as the strain rate further decreases to 0.00002 ps^{-1} , peak stress, critical strain, and steady flow stress decrease slightly compared to those values under the strain rate of 0.0002 ps^{-1} .

In order to explore the effects of strain rate on flow mechanism of G-phase, we employed von-Mises shear strain maps and BOOP (op-8) to characterize the atomistic structures after forming shear band, as shown in **Figures 7B–D** and **Figure 8**. The shear band has a width of $\sim 2.0 \text{ nm}$ under strain rates of

0.0002 ps^{-1} and 0.00002 ps^{-1} . It is $\sim 1 \text{ nm}$ narrower than the shear band formed under the strain rate of 0.002 ps^{-1} ($\sim 3 \text{ nm}$). These results indicate that a lower strain rate decreases the peak stress, the critical strain, the steady flow stress, and the width of the shear band for the G-phase. But when the strain rate decreases to $\sim 0.0002 \text{ ps}^{-1}$, the effects of strain rate on G-phase become negligible.

The Plasticity Mechanism of L-phase Under Shear Deformation

We now examine the shear deformation of the L-phase and compare to the G-phase. The equilibrium structure of the L-phase is characterized using the OP-8 at room temperature, as shown in **Figure 2B**. In contrast to the G-phase, the L-phase exhibits a more homogeneous structural character, which is consistent with the previous study (An et al., 2022). Next, a finite shear is applied to the L-phase. The predicted shear-stress-shear-strain relationship at room temperature is shown in **Figure 3**. The critical shear stress is $\sim 1.25 \text{ GPa}$, which is 1.57 GPa lower than for the G-phase. Moreover, the critical shear strain of L-phase is 0.10, also smaller than that of G-phase (0.15). Thus, the L-phase has a much lower yield stress and yield strain than the G-phase. The predicted shear modulus of L-phase from stress-strain curve (17.93 GPa) is also much lower than that of G-phase (29.97 GPa). The G-phase possesses higher strength, higher elastic modulus, and higher elastic strain limit.

The plasticity mechanism of L-phase was analyzed using atomic von-Mises strain, as shown in **Figure 9**. The intact structure before shear is shown in **Figure 9A**. With the shear strain increasing toward 0.1, the structure deforms elastically. At 0.1 shear strain, corresponding to the critical stress, some atoms show a slightly higher shear strain, suggesting that initiation of plasticity is not uniform on the atomic scale, as indicated by the speckle pattern in **Figure 9B**. With increasing shear strain up to 0.24, a shear band is formed and plastic flow becomes localized in the L-phase along shear direction. The initiation of the shear band relaxes the overall global shear

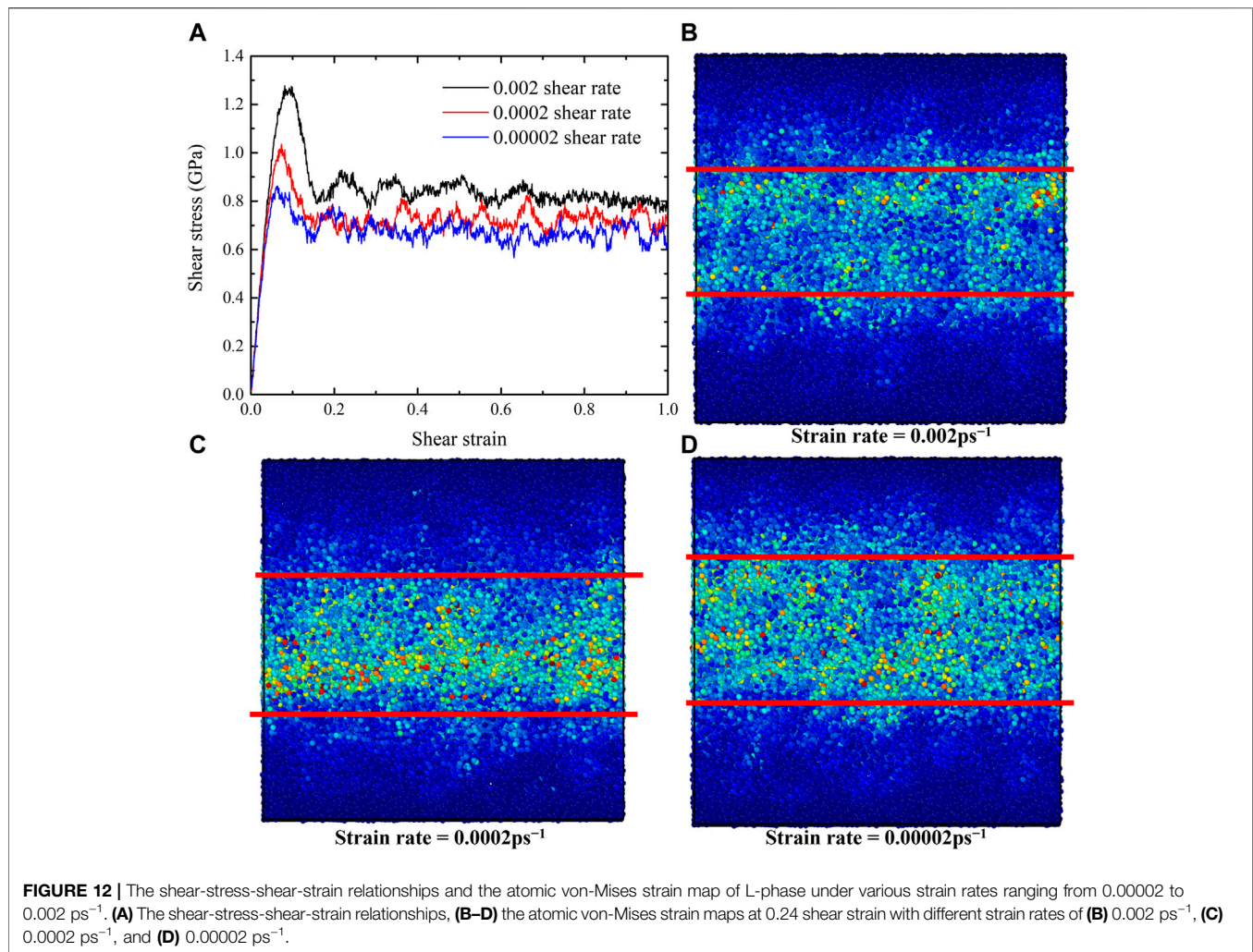


FIGURE 12 | The shear-stress-shear-strain relationships and the atomic von-Mises strain map of L-phase under various strain rates ranging from 0.00002 to 0.002 ps⁻¹. **(A)** The shear-stress-shear-strain relationships, **(B–D)** the atomic von-Mises strain maps at 0.24 shear strain with different strain rates of **(B)** 0.002 ps⁻¹, **(C)** 0.0002 ps⁻¹, and **(D)** 0.00002 ps⁻¹.

stress. In particular, at 0.24 shear strain, we observe that the shear band has a width of ~ 4 nm (**Figure 9C**). The global shear stress relaxes to ~ 0.8 GPa. This value is significantly lower than the final steady state stress for the G-phase (1.1 GPa), which is apparently related to the homogeneous structure of the L-phase versus the heterogeneous character of the G-phase. Heterogeneity may also explain why the shear band in L-phase is less spatially localized than in the G-phase. We also applied the BOOP analysis to investigate the local structural changes in the L-phase under the shear deformation. The OP-8 values for the initial structure and the structure after shear band formation are shown in **Figure 10**. Due to the homogeneous structural character of the L-phase, we see no obvious local atomic structural evolution within the shear band.

After obtaining the plasticity mechanism of L-phase, we also investigated the response of plastic-deformed L-phase during cyclic shear deformation. The obtained shear-stress-shear-strain relationship also exhibits typical Bauschinger effect, as shown in **Figure 11**. When shear along reversed or initial direction, the shear stress quickly flips back and reaches the

plastic flow with value of ~ 0.8 GPa. This phenomenon is similar to the response of G-phase under cyclic loading.

Summarizing, the homogeneous L-phase structure shows a significantly lower critical stress, a lower yield strain, and lower shear modulus compared to the G-phase. The plastic yielding of the L-phase under shear deformation is accompanied by formation of a shear band, which is similar to the case of the G-phase. However, the L-glass shear band is much less spatially localized than the shear band in the G-phase. This is apparently related to the homogeneous disordered structure of the L-phase. Moreover, in the L-phase glass no local atomic structural evolution is observed from the bond-orientational order parameters analysis. In addition, after the L-phase reaches the plastic flow, it also exhibits the Bauschinger effect under cyclic loading.

For the strain rate effects on shear deformation of L-phase, the shear-stress-shear-strain relationships under various strain rates are shown in **Figure 12A**. With the decrease of strain rate, both the critical shear stress and shear strain before plastic flow decreases, suggesting that the lower strain rate decreases the yield stress and yield strain of the L-phase. In addition, the

steady flow stress also decreases from ~ 0.8 GPa at strain rate of 0.002ps^{-1} to ~ 0.7 GPa at strain rate of 0.00002ps^{-1} . Considering the flow mechanism, a similar shear band with a width of ~ 4 nm forms under all three strain rates (**Figures 12B–D**). This suggests that plastic flow mechanism remains the same for L-phases under various strain rates.

CONCLUSION

In this study, we examine the binary Cu_2Zr system as a model system, applying MD simulations to illustrate the mechanical properties and shear deformation of both the G-phase and the L-phase. We find that the G-phase exhibits a higher critical shear stress, a higher elastic strain limit, and a higher shear modulus compared with the L-phase. The plastic yielding and flow of both the G-phase and L-phase are accompanied by spatial strain localization and shear band formation. For the heterogeneous G-phase, plasticity within the operating shear band is accompanied by local mechanical melting of the icosahedral-ordered core regions. Due to its heterogeneous structural character, the propagation of the shear band in the G-phase is inhibited by the surrounding hard-core regions. The shear bands in the plastic regime tend to localize in the disordered liquid like regions between the core regions. In contrast, the shear band formed in the L-phase is broader and more diffuse. We suggest that this is related to the more homogeneous disordered structural character of the L-phase. In addition, no apparent atomic level structural changes were observed with initiating the shear band in the L-phase case. It is also worth noting that Bauschinger effect under cyclic loading is observed in both G-phase and L-phase after reaching their state of plastic flow. Regarding the strain rate effects on shear deformation, we find that a lower strain rate decreases the

peak stress, the critical strain, and the steady flow stress for both G-phase and L-phase. For the plastic flow mechanism, at lower strain rates (0.0002ps^{-1} and 0.00002ps^{-1}), the shear band in G-phase is ~ 1 nm narrower than the shear band formed under the strain rate of 0.002ps^{-1} . In contrast, the formed shear band remains the same for L-phases under various strain rates. Our results imply that significant differences in mechanical properties should be observable for a heterogeneous configurationally ordered solid-like G-glass compared to a homogeneous L-glass having the same overall composition.

DATA AVAILABILITY STATEMENT

The original contributions presented in the study are included in the article/Supplementary material, further inquiries can be directed to the corresponding authors.

AUTHOR CONTRIBUTIONS

YS, WJ, KS, WG, and QA contributed to conception and design of the study. YS and QA performed the simulation. YS, WJ, KS, SC, WG, and QA performed the statistical analysis. YS wrote the first draft of the manuscript. All authors contribute to the edition of the manuscript.

FUNDING

WG was supported by gifts to the MSC. WJ and SC are supported by NSF grant with the award number DMR 1710744. KS is supported by the DFG, grant Sa337/10.

REFERENCES

- An, Q., Johnson, W. L., Samwer, K., Corona, S. L., and Goddard, W. A. (2020a). First-Order Phase Transition in Liquid Ag to the Heterogeneous G-phase. *J. Phys. Chem. Lett.* 11, 632–645. doi:10.1021/acs.jpcclett.9b03699
- An, Q., Johnson, W. L., Samwer, K., Corona, S. L., and Goddard, W. A. (2020b). Formation of Two Glass Phases in Binary Cu-Ag Liquid. *Acta Materialia* 195, 274–281. doi:10.1016/j.actamat.2020.05.060
- An, Q., Johnson, W. L., Samwer, K., Corona, S. L., and Goddard, W. A. (2021). The First Order L-G Phase Transition in Liquid Ag and Ag-Cu Alloys Is Driven by Deviatoric Strain. *Scripta Materialia* 194, 113695. doi:10.1016/j.scriptamat.2020.113695
- An, Q., Johnson, W. L., Samwer, K., Corona, S. L., Shen, Y., and Goddard, W. A. (2022). The L-G Phase Transition in Binary Cu-Zr Metallic Liquids. *Phys. Chem. Chem. Phys.* 24, 497–506. doi:10.1039/d1cp04157f
- Chen, L. Y., Setyawan, A. D., Kato, H., Inoue, A., Zhang, G. Q., Saida, J., et al. (2009). Free-Volume-Induced Enhancement of Plasticity in a Monolithic Bulk Metallic Glass at Room Temperature. *Scr. Mater.* 59, 75–78. doi:10.1016/j.scriptamat.2008.02.025
- Cheng, Y. Q., Ma, E., and Sheng, H. W. (2009). Atomic Level Structure in Multicomponent Bulk Metallic Glass. *Phys. Rev. Lett.* 102, 245501. doi:10.1103/PhysRevLett.102.245501
- Dai, L. H., and Bai, Y. L. (2008). Basic Mechanical Behaviors and Mechanics of Shear Banding in BMGs. *Int. J. Impact Eng.* 35, 704–716. doi:10.1016/j.ijimpeng.2007.10.007
- Frahsa, F., Bhattacharjee, A. K., Horbach, J., Fuchs, M., and Voigtmann, T. (2013). On the Bauschinger Effect in Supercooled Melts under Shear: Results from Mode Coupling Theory and Molecular Dynamics Simulations. *J. Chem. Phys.* 138, 12A513. doi:10.1063/1.4770336
- Greer, A. L., Cheng, Y. Q., and Ma, E. (2013). Shear Bands in Metallic Glasses. *Mater. Sci. Eng. R: Rep.* 74, 71–132. doi:10.1016/j.mser.2013.04.001
- Gu, X. J., Poon, S. J., and Shiflet, G. J. (2007). Mechanical Properties of Iron-Based Bulk Metallic Glasses. *J. Mater. Res.* 22, 344–351. doi:10.1557/jmr.2007.0036
- Hays, C. C., Kim, C. P., and Johnson, W. L. (2000). Microstructure Controlled Shear Band Pattern Formation and Enhanced Plasticity of Bulk Metallic Glasses Containing in situ Formed Ductile Phase Dendrite Dispersions. *Phys. Rev. Lett.* 84, 2901–2904. doi:10.1103/PhysRevLett.84.2901
- Karmakar, S., Lerner, E., and Procaccia, I. (2010). Plasticity-induced Anisotropy in Amorphous Solids: The Bauschinger Effect. *Phys. Rev. E* 82, 026104. doi:10.1103/PhysRevE.82.026104
- Ke, H. B., Wen, P., Peng, H. L., Wang, W. H., and Greer, A. L. (2011). Homogeneous Deformation of Metallic Glass at Room Temperature Reveals Large Dilatation. *Scripta Materialia* 64, 966–969. doi:10.1016/j.scriptamat.2011.01.047
- Klaumünzer, D., Lazarev, A., Maaß, R., Dalla Torre, F. H., Vinogradov, A., and Löffler, J. F. (2011). Probing Shear-Band Initiation in Metallic Glasses. *Phys. Rev. Lett.* 107, 185502. doi:10.1103/PhysRevLett.107.185502

- Lee, S.-C., Lee, C.-M., Lee, J.-C., Kim, H.-J., Shibutani, Y., Fleury, E., et al. (2008). Structural Disordering Process of an Amorphous alloy Driven by the Elastostatic Compression at Room Temperature. *Appl. Phys. Lett.* 92, 151906. doi:10.1063/1.2908218
- Lee, S. W., Huh, M. Y., Fleury, E., and Lee, J. C. (2006). Crystallization-Induced Plasticity of Cu-Zr Containing Bulk Amorphous Alloys. *Acta Mater.* 54, 349–355. doi:10.1016/j.actamat.2005.09.007
- Lewandowski, J. J., and Greer, A. L. (2006). Temperature Rise at Shear Bands in Metallic Glasses. *Nat. Mater.* 5, 15–18. doi:10.1038/nmat1536
- Li, W., Bei, H., Tong, Y., Dmowski, W., and Gao, Y. F. (2013). Structural Heterogeneity Induced Plasticity in Bulk Metallic Glasses: From Well-Relaxed Fragile Glass to Metal-like Behavior. *Appl. Phys. Lett.* 103, 171910. doi:10.1063/1.4827299
- Liu, Y. H., Wang, G., Wang, R. J., Zhao, D. Q., Pan, M. X., and Wang, W. H. (2007). Super Plastic Bulk Metallic Glasses at Room Temperature. *Science* 315, 1385–1388. doi:10.1126/science.1136726
- Maaß, R., Samwer, K., Arnold, W., and Volkert, C. A. (2014). A Single Shear Band in a Metallic Glass: Local Core and Wide Soft Zone. *Appl. Phys. Lett.* 105, 171902. doi:10.1063/1.4900791
- Mickel, W., Kapfer, S. C., Schröder-Turk, G. E., and Mecke, K. (2013). Shortcomings of the Bond Orientational Order Parameters for the Analysis of Disordered Particulate Matter. *J. Chem. Phys.* 138, 044501. doi:10.1063/1.4774084
- Na, J. H., Corona, S. L., Hoff, A., and Johnson, W. L. (2020). Observation of an Apparent First-Order Glass Transition in Ultrafragile Pt-Cu-P Bulk Metallic Glasses. *Proc. Natl. Acad. Sci. U.S.A.* 117, 2779–2787. doi:10.1073/pnas.1916371117
- Patinet, S., Barbot, A., Lerbinger, M., Vandembroucq, D., and Lemaître, A. (2020). Origin of the Bauschinger Effect in Amorphous Solids. *Phys. Rev. Lett.* 124, 205503. doi:10.1103/PhysRevLett.124.205503
- Pedersen, O. B., Brown, L. M., and Stobbs, W. M. (1981). The Bauschinger Effect in Copper. *Acta Metallurgica* 29, 1843–1850. doi:10.1016/0001-6160(81)90110-3
- Pekarskaya, E., Kim, C. P., and Johnson, W. L. (2001). *In Situ* transmission Electron Microscopy Studies of Shear Bands in a Bulk Metallic Glass Based Composite. *J. Mater. Res.* 16, 2513–2518. doi:10.1557/JMR.2001.0344
- Plimpton, S. (1995). Fast Parallel Algorithms for Short-Range Molecular Dynamics. *J. Comput. Phys.* 117, 1–19. doi:10.1006/jcph.1995.1039
- Schroers, J., and Johnson, W. L. (2004). Ductile Bulk Metallic Glass. *Phys. Rev. Lett.* 93, 255506. doi:10.1103/PhysRevLett.93.255506
- Schuh, C., Hufnagel, T., and Ramamurty, U. (2007). Mechanical Behavior of Amorphous Alloys. *Acta Materialia* 55, 4067–4109. doi:10.1016/j.actamat.2007.01.052
- Shen, J., Lu, Z., Wang, J. Q., Lan, S., Zhang, F., Hirata, A., et al. (2020). Metallic Glacial Glass Formation by a First-Order Liquid-Liquid Transition. *J. Phys. Chem. Lett.* 11, 6718–6723. doi:10.1021/acs.jpcllett.0c01789
- Shimizu, F., Ogata, S., and Li, J. (2007). Theory of Shear Banding in Metallic Glasses and Molecular Dynamics Calculations. *Mater. Trans.* 48, 2923–2927. doi:10.2320/matertrans.MJ200769
- Spaepen, F. (2006). Homogeneous Flow of Metallic Glasses: A Free Volume Perspective. *Scripta Materialia* 54, 363–367. doi:10.1016/j.scriptamat.2005.09.046
- Steinhardt, P. J., Nelson, D. R., and Ronchetti, M. (1983). Bond-orientational Order in Liquids and Glasses. *Phys. Rev. B* 28, 784–805. doi:10.1103/PhysRevB.28.784
- Stukowski, A. (2010). Visualization and Analysis of Atomistic Simulation Data with OVITO-The Open Visualization Tool. *Model. Simul. Mater. Sci. Eng.* 18, 015012. doi:10.1088/0965-0393/18/1/015012
- Sun, Y. H., Louzguine-Luzgin, D. V., Ketov, S., and Greer, A. L. (2014). Pure Shear Stress Reversal on a Cu-Based Bulk Metallic Glass Reveals a Bauschinger-type Effect. *J. Alloys Compd.* 615, S75–S78. doi:10.1016/j.jallcom.2013.11.104
- Szuecs, F., Kim, C. P., and Johnson, W. L. (2001). Ductile Phase Reinforced Bulk Metallic Glass Composite. *Acta Mater.* 49, 1507–1513. doi:10.1016/S1359-6454(01)00068-4
- Tang, C., Peng, H., Chen, Y., and Ferry, M. (2016). Formation and Dilatation of Shear Bands in a Cu-Zr Metallic Glass: A Free Volume Perspective. *J. Appl. Phys.* 120, 235101. doi:10.1063/1.4972189
- Tucker, G. J., Zimmerman, J. A., and McDowell, D. L. (2011). Continuum Metrics for Deformation and Microrotation from Atomistic Simulations: Application to Grain Boundaries. *Int. J. Eng. Sci.* 49, 1424–1434. doi:10.1016/j.ijengsci.2011.03.019
- Urata, S., and Li, S. (2018). A Multiscale Shear-Transformation-Zone (STZ) Model and Simulation of Plasticity in Amorphous Solids. *Acta Materialia* 155, 153–165. doi:10.1016/j.actamat.2018.05.058
- Wang, W. H., Yang, Y., Nieh, T. G., and Liu, C. T. (2015). On the Source of Plastic Flow in Metallic Glasses: Concepts and Models. *Intermetallics* 67, 81–86. doi:10.1016/j.intermet.2015.08.004
- Wu, Y., Cao, D., Yao, Y., Zhang, G., Wang, J., Liu, L., et al. (2021). Substantially Enhanced Plasticity of Bulk Metallic Glasses by Densifying Local Atomic Packing. *Nat. Commun.* 12, 6582. doi:10.1038/s41467-021-26858-9
- Yang, B., Morrison, M. L., Liaw, P. K., Buchanan, R. A., Wang, G., Liu, C. T., et al. (2005). Dynamic Evolution of Nanoscale Shear Bands in a Bulk-Metallic Glass. *Appl. Phys. Lett.* 86, 141904. doi:10.1063/1.1891302
- Yang, B., Liu, C. T., Nieh, T. G., Morrison, M. L., Liaw, P. K., and Buchanan, R. A. (2006). Localized Heating and Fracture Criterion for Bulk Metallic Glasses. *J. Mater. Res.* 21, 915–922. doi:10.1557/jmr.2006.0124
- Yang, Y. J., Cheng, B. Y., Lv, J. W., Li, B., Ma, M. Z., Zhang, X. Y., et al. (2019). Effect of Ag Substitution for Ti on Glass-Forming Ability, thermal Stability and Mechanical Properties of Zr-Based Bulk Metallic Glasses. *Mater. Sci. Eng. A* 746, 229–238. doi:10.1016/j.msea.2018.12.123
- Yue, X., Brechtel, J., Wang, F., Chang, Z., Liaw, P. K., and Fan, C. (2020). Deformation Behavior of Annealed Cu64Zr36 Metallic Glass via Molecular Dynamics Simulations. *Mater. Des.* 191, 108660. doi:10.1016/j.matdes.2020.108660

Conflict of Interest: The authors declare that the research was conducted in the absence of any commercial or financial relationships that could be construed as a potential conflict of interest.

Publisher's Note: All claims expressed in this article are solely those of the authors and do not necessarily represent those of their affiliated organizations, or those of the publisher, the editors and the reviewers. Any product that may be evaluated in this article, or claim that may be made by its manufacturer, is not guaranteed or endorsed by the publisher.

Copyright © 2022 Shen, Johnson, Samwer, Corona, Goddard and An. This is an open-access article distributed under the terms of the Creative Commons Attribution License (CC BY). The use, distribution or reproduction in other forums is permitted, provided the original author(s) and the copyright owner(s) are credited and that the original publication in this journal is cited, in accordance with accepted academic practice. No use, distribution or reproduction is permitted which does not comply with these terms.